



**HAL**  
open science

# Removable Composite Electrode Made of Silver Nanoparticles on Pyrolyzed Photoresist Film for the Electroreduction of 4-Nitrophenol

Maxime Puyo, Pierre Fau, Myrtil L. Kahn, David Mesguich, Jérôme Launay,  
Katia Fajerweg

► **To cite this version:**

Maxime Puyo, Pierre Fau, Myrtil L. Kahn, David Mesguich, Jérôme Launay, et al.. Removable Composite Electrode Made of Silver Nanoparticles on Pyrolyzed Photoresist Film for the Electroreduction of 4-Nitrophenol. *Langmuir*, 2019, 35 (44), pp.14194-14202. 10.1021/acs.langmuir.9b02405 . hal-02388677

**HAL Id: hal-02388677**

**<https://hal.science/hal-02388677v1>**

Submitted on 6 Oct 2020

**HAL** is a multi-disciplinary open access archive for the deposit and dissemination of scientific research documents, whether they are published or not. The documents may come from teaching and research institutions in France or abroad, or from public or private research centers.

L'archive ouverte pluridisciplinaire **HAL**, est destinée au dépôt et à la diffusion de documents scientifiques de niveau recherche, publiés ou non, émanant des établissements d'enseignement et de recherche français ou étrangers, des laboratoires publics ou privés.








## Open Archive Toulouse Archive Ouverte (OATAO)

OATAO is an open access repository that collects the work of Toulouse researchers and makes it freely available over the web where possible

This is an author's version published in: <http://oatao.univ-toulouse.fr/26614>

**Official URL:** <https://doi.org/10.1021/acs.langmuir.9b02405>

### To cite this version:

Puyo, Maxime  and Fau, Pierre  and Kahn, Myrtil  and Mesguich, David  and Launay, Jérôme and Fajerweg, Katia  *Removable Composite Electrode Made of Silver Nanoparticles on Pyrolyzed Photoresist Film for the Electroreduction of 4-Nitrophenol*. (2019) *Langmuir*, 35 (44). 14194-14202. ISSN 0743-7463

Any correspondence concerning this service should be sent to the repository administrator: [tech-oatao@listes-diff.inp-toulouse.fr](mailto:tech-oatao@listes-diff.inp-toulouse.fr)

# Removable Composite Electrode Made of Silver Nanoparticles on Pyrolyzed Photoresist Film for the Electroreduction of 4-Nitrophenol

Maxime Puyo,<sup>†</sup> Pierre Fau,<sup>\*,†</sup> Myrtil L. Kahn,<sup>†</sup> David Mesguich,<sup>‡</sup> Jérôme Launay,<sup>§</sup> and Katia Fajerwerg<sup>\*,†</sup>

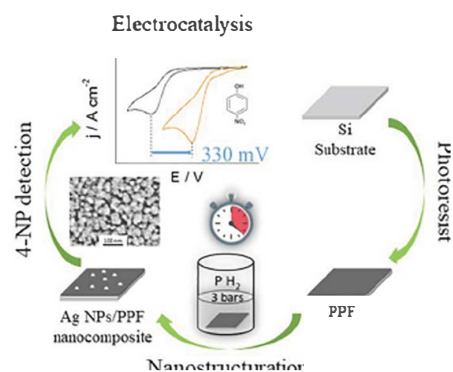
<sup>†</sup>LCC–CNRS, University of Toulouse, 205 route de Narbonne, F 31077 Toulouse, France

<sup>‡</sup>CIRIMAT, University of Toulouse, CNRS, Université Toulouse 3 Paul Sabatier, 118 route de Narbonne, F 31062 Toulouse cedex 9, France

<sup>§</sup>LAAS CNRS, University of Toulouse, 7 avenue du colonel Roche, F 31077 Toulouse, France

## Supporting Information

**ABSTRACT:** Access to removable nanocomposite electrodes for electroensing of pollutants is of great importance. However, the preparation of reproducible and reliable carbon electrodes decorated with metallic nanoparticles, a prerequisite for trustworthy devices, remains a challenge. Here we describe an innovative and easy method to prepare such electrodes. These latter are silicon coated with a thin carbon film on which controlled silver nanostructures are grafted. Different silver nanostructures and surface coverage of the carbon electrode (16, 36, 51, and 67%) can be obtained through a careful control of the time of the hydrogenolysis of the N–N' isopropyl butylamidinate silver organometallic precursor ( $t = 1, 5, 15,$  and  $60$  min, respectively). Importantly, all nanocomposite surfaces are efficient for the electroreduction of 4 nitrophenol with a remarkable decrease of the overpotential of the reduction of such molecule up to  $330$  mV. The surfaces are characterized by atomic force microscopy, grazing incidence X ray diffraction, scanning electronic microscopy, and Raman spectroscopy. Furthermore, surface enhanced Raman scattering effect is also observed. The exaltation of the Raman intensity is proportional to the surface coverage of the electrode; the number of hot spots increases with the surface coverage.



## INTRODUCTION

Nanocomposites materials (metallic, metal oxides nanoparticles (NPs), carbon nanotubes, matrixes, etc.) offer new opportunities thanks to the synergetic combination of the physical and chemical properties of each component.<sup>1–6</sup> Metallic nanoparticles (Au, Ag, Pt, etc.) present interesting optical and electronic properties and potential utility in (electro)catalysis.<sup>7,8</sup> Among these noble metallic NPs, silver is particularly attractive because of its low cost, high electrical conductivity, and (electro)catalytic activity.<sup>2,9,10</sup> The specific activity of Ag catalysts is strongly related to their morphology and size distribution.<sup>11</sup> Ag nanoparticles (AgNPs) with small size (typically less than ca. 20 nm) and narrow size distribution are ideal for high (electro)catalytic activity owing to their large surface to volume ratio.<sup>12–18</sup> However, the integration of well controlled nano objects on substrates remains a challenge for addressing new sensing devices and scaling up issues in nanotechnology.<sup>12</sup> For instance, grafting AgNPs on various well defined surfaces, a key step process for electro analysis and catalysis, still remains difficult to master.<sup>10,16,19–22</sup>

A number of methods have been described to deposit NPs on flat surfaces, as recently reported.<sup>23–25</sup> Simple deposition methods of presynthesized colloidal suspensions of AgNPs on any substrate (silicon, carbon, metallic substrates, etc.) are

largely used as cost efficient techniques.<sup>26,27</sup> These straightforward methods often lead to poor and random control of the NPs surface distribution. To better position and graft the NPs, more sophisticated techniques have been proposed, by combining simple (electro)deposition methods with well defined surfaces and/or control of the surface chemistry.<sup>9,16,28–30</sup> For instance, the functionalization of both substrate and particles can enhance their adhesion using specific molecules such as DNA, self assembly monolayers (SAMs),<sup>31,32</sup> covalent attachment of molecular species via electro grafting of diazonium salts, etc.<sup>33–36</sup>

The deposition of nanoparticles on an oxide support has also been achieved by the solution grafting of metalorganic precursors followed by thermal reduction under reducing atmosphere. This technique is well adapted for the generation of very small nanoparticles (<1 nm mean size) for heterogeneous catalysis applications with Pt–Sn, Ru, or Ir catalytic material.<sup>37,38</sup> More recently, we described a new chemical process where metal amidinate based precursors are directly decomposed by thermal hydrogenation in solution in

the presence of the substrate to be covered.<sup>39</sup> The hydrolysis of the precursor generates a colloidal solution of metastable nanoparticles stabilized by the amidine ligands. Because of the poor stabilization by the ancillary ligand, the nanoparticles undergo with time a deposition mechanism on all the immersed surfaces. This process gives rise to the decoration of the substrate with metallic nanoparticles, which can be controlled through the conditions of the hydrogenolysis reaction.<sup>40</sup>

Carbon based electrodes are commonly used for their large potential range and chemical inertness. However, such electrodes require long processing time, and the resulting surfaces are very often difficult to reproduce, especially because of the polishing process. To overcome these drawbacks, pyrolyzed photoresist films (PPF) made from the pyrolysis of carbon rich polymers uniformly coated onto Si wafers provide straightforward smooth near atomically flat surfaces with similar electrochemical behavior as glassy carbon electrodes (GCE).<sup>14,34,41,42</sup> Up to now, very few works are devoted to the decoration of planar removable PPF substrates with controlled NPs for the development of electrochemical sensors.<sup>15,43</sup>

4 Nitrophenol (4 NP) is a hazardous substance that can have a major environmental impact due to its toxicity and persistence. It is one of the nitrophenols included in the U.S. Environmental Protection Agency List of Priority Pollutants.<sup>16,20,44</sup> In this paper, we present a complete design process for a removable device allowing the electro detection of 4 NP. This device is based on PPF surfaces (1 × 1 cm) decorated with controlled AgNPs nanostructures. Atomically flat surfaces of PPF will ensure a very reproducible substrate, which is necessary for a reliable decoration with Ag nanoparticles. Herein N–N' isopropyl butylamidinate silver, [Ag(Bu amd)], is synthesized and used as the metalorganic precursor for the AgNPs preparation. Their direct deposition on the PPF surfaces is achieved during the hydrogenolysis of the precursor. This deposition is monitored at different times ( $t = 1, 5, 15,$  and  $60$  min), and the corresponding nanocomposite AgNPs/PPF electrode is characterized by atomic force microscopy (AFM), X ray diffraction (XRD), grazing incidence X ray diffraction (GIXRD), scanning electronic microscopy (SEM), and Raman spectroscopy. Very distinct and reproducible AgNPs structures are obtained on the PPF surfaces, leading to efficient electrochemically active surfaces. All AgNPs/PPF interfaces present an electro catalytic behavior compared to a bare PPF surface. Particularly, 15 and 60 min AgNPs structures on PPF reveal a high number of optically active hot spots leading to an exaltation of the Raman signal, which is, concomitantly, correlated to the optimum electrocatalytic activity for the reduction of 4 NP molecule. This detection feature may pave the way for the building of a device using both electrochemical and optical detection system.

## ■ EXPERIMENTAL SECTION

**Reagents.** Toluene and *n* pentane were obtained from a solvent purification system (Braun) and were further dried on a molecular sieve 4 Å, 4–8 mesh purchased from Sigma Aldrich Company. *N,N'* Diisopropylcarbodiimide (99%) and *n* butyllithium (2.5 mol L<sup>-1</sup> in hexane) were purchased from Sigma Aldrich Company, and AgCl (99.00%) was purchased from Strem Company; the AZ 5214E Photoresist resin was purchased from MicroChemicals Company. Phosphate buffer was made from NaH<sub>2</sub>PO<sub>4</sub> (Analytical grade, Fischer Chemical), NaOH (Analytical grade, Acros Organics), and Milli Q water. 4 Nitrophenol (Analytical grade) was purchased from Sigma

Aldrich Company. Precursors and solvent were stored in a glovebox to avoid any traces of moisture and oxygen. The silver precursor [Ag(Bu amd)] synthesis (Supporting Information, SI 1 and Scheme S1) and its use was carried on in an inert atmosphere (Ar atmosphere, using either glovebox or standard Fischer–Porter techniques), with oven dried glassware protected from light.

**Preparation of the Pyrolyzed Photoresist Film Surfaces.** A one side polished 2 × 2 cm doped silicon substrate, Si(100), was cleaned by a Piranha solution, thoroughly rinsed with deionized water, and dried in a nitrogen flow. The native silicon oxide layer was removed with a HF solution (5%, in deionized water) and then rinsed with deionized water and dried in a nitrogen flow.

In clean room conditions, 110 μL of the AZ 5214E Photoresist resin was spin coated on the silicon substrate (1000 rpm for 30 s, 3000 rpm for 30 s). The film was soft baked at 130 °C for 30 min, and then a second layer of photoresist was spin coated in the same conditions. The final film was ca. 4 μm thick before the pyrolysis in a 5% H<sub>2</sub>/Ar gas flow (30 L·h<sup>-1</sup>). The heating protocol is derived from the one used by K. Ounnunkad et al.<sup>45</sup> (Supporting Information, SI 2).

Before the AgNPs deposition on PPF surfaces, the PPF silicon substrates were cleaved as 1 × 1 cm samples.

**Deposition of AgNPs(t) on PPF Surfaces.** A 1 × 1 cm PPF silicon substrate was placed in a Fisher Porter (FP) reactor (PPF surface facing the bottom of the bottle). Five milliliters of a [Ag(Bu amd)] solution (2 mmol L<sup>-1</sup>, 0.6 mg mL<sup>-1</sup>, in toluene) was introduced in the FP tube. The reactor was heated without stirring at 60 °C for 5 min; no color change of the solution was observed at this stage. Then, the reactor was pressurized with 3 bar of H<sub>2</sub> for a duration  $t$ . At the end of  $t$ , the tube was quickly purged from H<sub>2</sub> and backfilled with Ar. To ensure the quenching of the reaction, the reactor was placed in an ice bath. The color of the resulting solution varied depending on the reaction time. After 1 min, the solution was pale orange. After 5 min, the solution was orange (reactor walls covered with a light blue Ag NPs film). After 15 min, the solution was orange (reactor walls covered with a silver mirror). After 60 min, the solution was yellow (reactor walls covered with a silver mirror).

The unreacted remaining [Ag(Bu amd)] was removed from the substrate by washing it with a flow of 10 mL of toluene. The AgNPs (t)/PPF was dried and stored in the freezer of the glovebox.

**Electrochemical Measurements.** All solutions were prepared from suprapure chemicals and Milli Q water. Measurements were performed using a Metrohm potentiostat (PGSTAT N302) controlled with GPES software. The experiments were performed at room temperature in a compact three electrode cell ( $V = 1.2$  mL), with a reference electrode (Ag/AgCl/KCl 3 mol L<sup>-1</sup>) and a platinum wire as counter electrode (Supporting Information, Scheme S2). All potentials were reported with respect to the reference electrode.

Working electrodes PPF/Si ( $d = 5.7$  mm,  $A = 25.5$  mm<sup>2</sup>), AgNPs (t)/PPF of this study were compared with silver thin film electrode ( $d = 5.7$  mm,  $A = 25.5$  mm<sup>2</sup>) prepared by physical vapor deposition (PVD) on Si substrate (LAAS facilities) (Supporting Information, SI 5).

All the electrodes were used for CV measurements directly after preparation. They were carefully rinsed using Milli Q water and directly immersed in a deaerated 5 × 10<sup>-4</sup> mol·L<sup>-1</sup> 4 NP phosphate buffer solution by running five scans between -0.1 and -1.1 V at a scan rate of 100 mV s<sup>-1</sup> for stabilization. The PVD Ag/Si electrodes, (PVD Ag films) as well as the AgNP/PPF ones, were used for CV measurements directly after preparation. The potential window of these electrodes is -0.8 ≤  $E$  (V) ≤ 0.3 and -1.1 ≤  $E$  (V) ≤ 0.3 respectively. All the AgNPs/PPF electrodes were carefully rinsed using Milli Q water and directly immersed in a deaerated 0.5 mmol·L<sup>-1</sup> 4 NP phosphate buffer solution by running five scans between -0.1 and -1.0 V at a scan rate of 100 mV·s<sup>-1</sup> for stabilization. For PVD Ag films, the same procedure was applied with a potential range from -0.1 to -0.8 V. The geometrical surface area  $A$  of the working electrode was used to calculate current density  $j$ .

**Characterizations.** The nuclear magnetic resonance (NMR) characterization of the silver precursor was done using a 1 mmol L<sup>-1</sup>

solution of  $[\text{Ag}(\text{Bu amd})]$  ( $0.3 \text{ g L}^{-1}$ , in dry toluene  $d_8$ ) solution analyzed by a Bruker Advance 400 spectrometer.

**XRD.** An X ray diffractometer PANalytical X'Pert PRO with  $\text{Cu K}\alpha_1, \text{K}\alpha_2$  radiation ( $\lambda = 1.54059, 1.54442 \text{ \AA}$ ) was used. To increase the signal from the thin films and minimize the effect of the substrate, the GIXRD method was used. Data collection was performed on the  $2^\circ < 2\theta < 80^\circ$  angular range with a step size of  $0.017^\circ$  for XRD and on the  $30^\circ < 2\theta < 80^\circ$  angular range with a step size of  $0.03^\circ$  for GIXRD. The grazing angle was set at  $0.4^\circ\text{--}0.5^\circ$  for all samples measured by GIXRD except for GIXRD Ag/Si, which was measured with a grazing angle of  $1.5^\circ$ .

SEM images of PPF/Si and AgNPs(t)/PPF were obtained using an SEM FEG Jeol JSM 7800F.

Transmission electron microscopy (TEM) images of AgNPs in the supernatant were obtained using a Jeol 1011 transmission electron microscope operating at 120 kV.

AFM images were obtained using a Smarts SPM 1000, AIST NT apparatus.

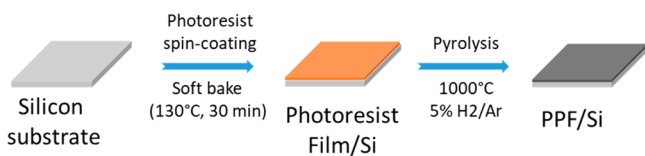
The nanoparticle size distributions were determined from SEM images by measuring a minimum of 200 particles of each sample. They were analyzed by the two dimensional (2D) plot method (details are given in Supporting Information, SI 4). This method is very useful to probe the correlation between width and length for the shape analysis of anisotropic nanoparticles.<sup>46</sup> The mean diameter and standard deviation are evaluated by fitting of the histogram with a Gaussian curve. 95% confidence intervals were given (i.e., twice the standard deviation of the Gaussian distribution or  $\sim 0.849$  the width of the peak at half height).

The Raman spectra of the PPF and AgNPs(t)/PPF surfaces were recorded using a microspectrometer (Xplora, Horiba) with a  $\lambda = 532 \text{ nm}$  laser (intensity  $0.1 \text{ mW}$  for PPF and  $0.01 \text{ mW}$  AgNPs(t)/PPF surfaces) focused with a  $50\times$  objective (numeric aperture = 0.5).

## RESULTS AND DISCUSSION

**Preparation and Characterization of PPF.** The different steps of the preparation of the PPF surfaces are presented Scheme 1. PPF samples are prepared by spin coating a

**Scheme 1. Schematic Preparation Protocol of the PPF on a Silicon Substrate**



photoresist resin (AZ 5214E) onto a  $750 \mu\text{m}$  thick doped silicon substrate with an average sheet resistivity of  $0.01\text{--}0.05 \Omega\cdot\text{cm}^{-1}$ . The carbon film pyrolysis procedure at  $1000^\circ\text{C}$  under a  $5\% \text{ H}_2/\text{Ar}$  is detailed in Supporting Information, SI 2. This procedure yields a well defined film with a reproducible thickness of  $0.8 \mu\text{m}$  measured from the cross sectional view of the layer by SEM (Supporting Information, Figure S2). PPF surfaces are very homogeneous and crack free (Supporting Information, Figure S3). Additionally, the root mean square roughness (rms) determined from AFM measurements is typically less than  $0.5 \text{ nm}$  indicating that these PPF surfaces present a near atomically flat surface (Supporting Information, Figure S4). The X ray diffractogram of PPF (Supporting Information, Figure S5) does not present any peak in accordance with an amorphous graphite and/or carbon films with crystallites size lower than  $10 \text{ nm}$ .

Typical Raman spectrum of the as obtained PPF surfaces is presented in Figure 1. Two main bands are present, respectively, at ca.  $1345 \text{ cm}^{-1}$  (D band) and  $1600 \text{ cm}^{-1}$  (G

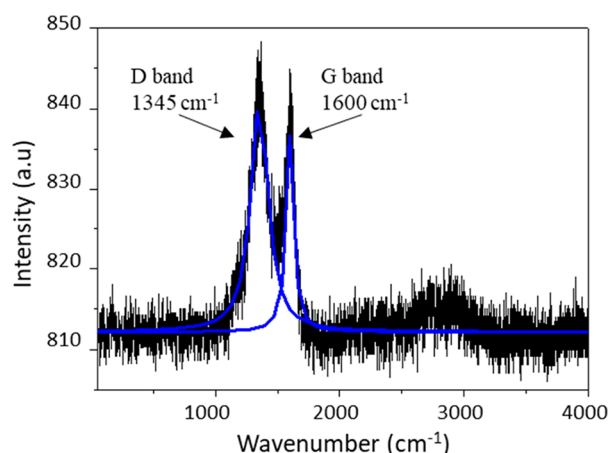
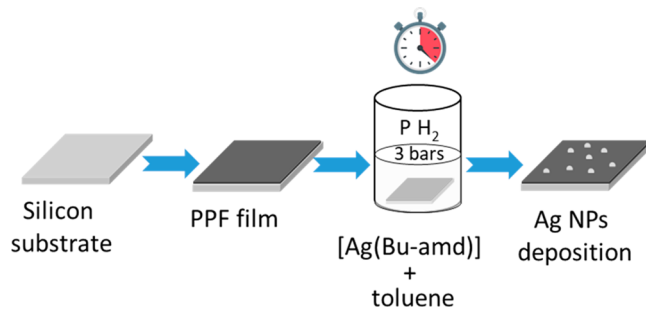


**Figure 1.** Raman spectrum of PPF (green laser,  $\lambda = 532 \text{ nm}$ ). Deconvoluted spectra as Lorentzian functions (blue line).

band). The fitting of this spectrum leads to D lines assigned to defects in the carbon layer, and to G lines corresponding to the graphitic structure of  $\text{sp}^2$  carbon, with  $\text{E}_{2g}$  phonons and breathing mode of K point phonons of  $\text{A}_{1g}$ , respectively.<sup>22,47</sup> The broad peak in the  $2500$  to  $3000 \text{ cm}^{-1}$  region corresponds to the harmonic combination of D and G bands. On the basis of the Ferrari and Robertson's model,<sup>48</sup> the PPF of our study presents an area ratio of the D and G bands close to 2.7, which indicates a rather large number of defects compared to the well organized graphitic carbon domains.

**Decoration of the PPF with Silver NPs.** The formation of AgNPs on PPF was achieved through the thermal hydrogenolysis of the  $[\text{Ag}(\text{Bu amd})]$  precursor (Supporting Information, Scheme S1 and Figure S1). In this process (Scheme 2), the PPF substrate was directly placed inside a

**Scheme 2. Schematic Description of the Process Steps for the Decoration of PPF with AgNPs**



reactor containing the precursor solubilized in toluene. The reactor was placed in an oil bath at  $60^\circ\text{C}$ , and the decomposition of the precursor started when the reactor was pressurized with 3 bar of  $\text{H}_2$ . The process yields AgNPs in solution, which spontaneously deposit on all immersed surfaces including the PPF ones.<sup>40</sup> The amount of AgNPs collected on the surface was directly proportional to the time of hydrogenolysis.

The decomposition stages by thermal hydrogenolysis of a copper amidinate precursor, a structural analogue of the silver amidinate precursor, has recently been highlighted.<sup>39</sup> The hydrogenolysis of metal amidinates in solution produces the colloidal nucleation of metallic NPs. Importantly, the NPs are temporarily maintained in solution thanks to the amidine

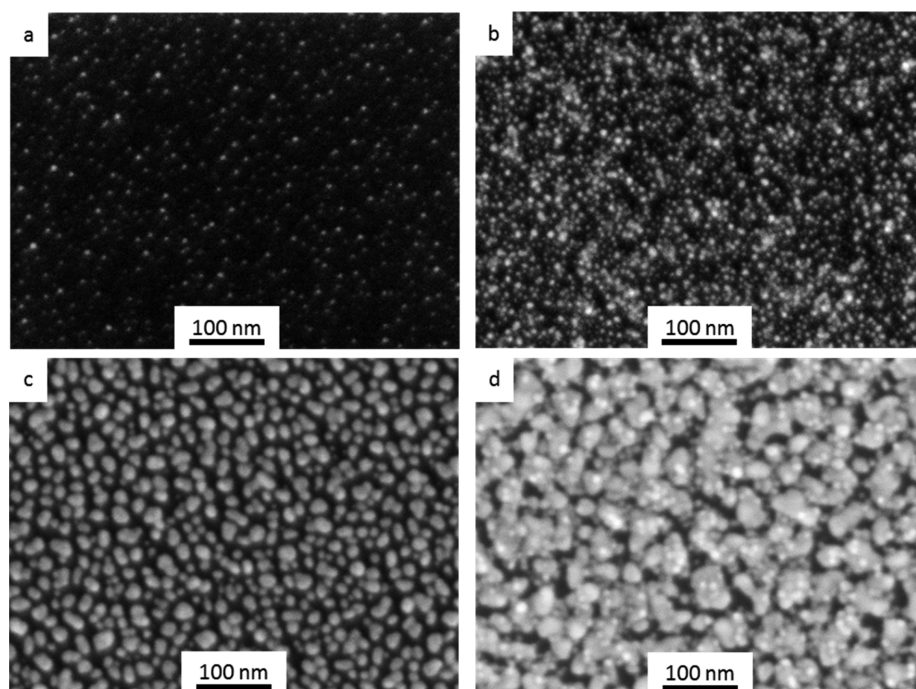


**Figure 2.** SEM images of PPF films decorated with AgNPs(1 min) (a); AgNPs(5 min) (b); AgNPs(15 min) (c); AgNPs(60 min) (d).

moieties released by the decomposition of the precursor. However, this stabilization is only weak; the NPs are in a metastable state and tend to (i) aggregate in solution and (ii) deposit on immersed surface (reactor walls, substrate) over time. If the process is allowed to evolve up to the full consumption of the precursor, a continuous metallic layer forms on surfaces. A similar mechanism is expected in the case of the silver amidinate precursor. Thus, we hypothesized that the coverage of the PPF surfaces by the AgNPs can be varied in a controlled way by appropriately changing the time of hydrogenolysis. Therefore, PPF samples with a time of deposition of 1, 5, 15, and 60 min were prepared.

#### SEM Characterization of AgNPs(t)/ PPF Surfaces.

Figure 2 shows typical SEM images of the PPF substrates decorated with AgNPs for 1, 5, 15, and 60 min of hydrogenolysis. At 1 min, the formation of isolated AgNPs is observed. Remarkably, the mean size of the AgNPs is  $\sim 6$  ( $\pm 1$ ) nm, and the particles are homogeneously distributed on the whole PPF surface (Figure 2a, Table 1). Each Ag NP is separated from the neighboring one by at least several tens of

nanometers. It is worth noting that the size of the NPs deposited on the substrate is very close to the mean size of the NPs found in the supernatant and analyzed by TEM ( $4.7$  ( $\pm 2.9$ ) nm) (Supporting Information, Figure S6a). As expected, at 5 min, the number of AgNPs on the substrate increases, and few aggregates are observed (Figure 2b). A mean size of  $7$  ( $\pm 2$ ) nm is obtained (Table 1). The image analysis using a contrast detection tool (ImageJ software) indicates a surface coverage of the substrate of  $16$  ( $\pm 3$ ) % after 1 min of deposition and  $36$  ( $\pm 4$ ) % after 5 min.

When the deposition time is increased to 15 min, a different microstructure appears on the PPF. In that case, the NPs present a molten aspect, and some of them display an anisotropic shape. The image analysis reveals a surface coverage close to  $51$  ( $\pm 2$ ) % showing two kinds of population. The size analysis of these NPs performed through a recently developed 2D plot<sup>46</sup> indicates that anisotropic aggregates of  $20$  ( $\pm 3$ )  $\times$   $14$  ( $\pm 3$ ) nm, accounting for 57% of the population, and isotropic NPs of  $11$  ( $\pm 2$ ) nm, accounting for 43% of the population, are present on the substrate (Table 1). One of the main advantages of such a 2D plot comes from the multivariate analysis of the data that enables to isolate the subpopulations and to obtain more accurate quantitative values for each one (proportion, average length and width, and correlation). The correlation values for these two identified subpopulations are similar and close to 0.74 indicating a strong correlation between the length and the width. Interestingly, the particles present in the supernatant after 15 min of reaction are still isotropic, and their mean size is  $5.5$  ( $\pm 2.8$ ) nm (Supporting Information, Figure S6b). This suggests that the AgNPs continuously nucleate in solution and regularly deposit on the already adsorbed AgNPs over time, leading to the growth of large aggregates with an elongated shape. The same 2D plot analysis performed for the deposition times of 1 and 5 min shows a collection of points centered along the median line (Supporting Information, Figure S7a,b) in agreement with isotropic AgNPs. The multivariate analysis confirms the

**Table 1. Cathodic Peak Potential ( $E_p$ ) and Structural Data of the Silver Nanoparticles (AgNPs) Deposited on PPF Surface**

working electrode	$E_p$ /V vs Ag/AgCl/Cl <sup>-</sup>	size <sup>a</sup> /nm	surface coverage <sup>b</sup> /%
PPF surface	0.837 ( $\pm 0.009$ )		0
AgNPs(1 min)/PPF	0.825 ( $\pm 0.016$ )	6 ( $\pm 1$ )	16 ( $\pm 3$ )
AgNPs(5 min)/PPF	0.803 ( $\pm 0.013$ )	7 ( $\pm 2$ )	36 ( $\pm 4$ )
AgNPs(15 min)/PPF	0.507 ( $\pm 0.011$ )	20 ( $\pm 3$ ) $\times$ 14 ( $\pm 3$ ) 11 ( $\pm 2$ )	51 ( $\pm 2$ )
AgNPs(60 min)/PPF	0.506 ( $\pm 0.016$ )	35 ( $\pm 11$ ) $\times$ 22 ( $\pm 6$ ) 8 ( $\pm 1$ )	67 ( $\pm 3$ )

<sup>a</sup>Determined from SEM images. <sup>b</sup>Determined from 2D plot analysis.

presence of one single population with a mean size of ca. 6 nm. Finally, after 60 min, the evolution of the growth of the aggregates present on the PPF as well as the increasing surface coverage are confirmed. In these conditions, a shiny metallic mirror appears on all the immersed part of the reactor. The image analysis reveals a surface coverage close to 67 ( $\pm 3$ ) % with still a bimodal distribution of AgNPs. The 2D plot analysis of these AgNPs (Figure 3a) indicates that anisotropic

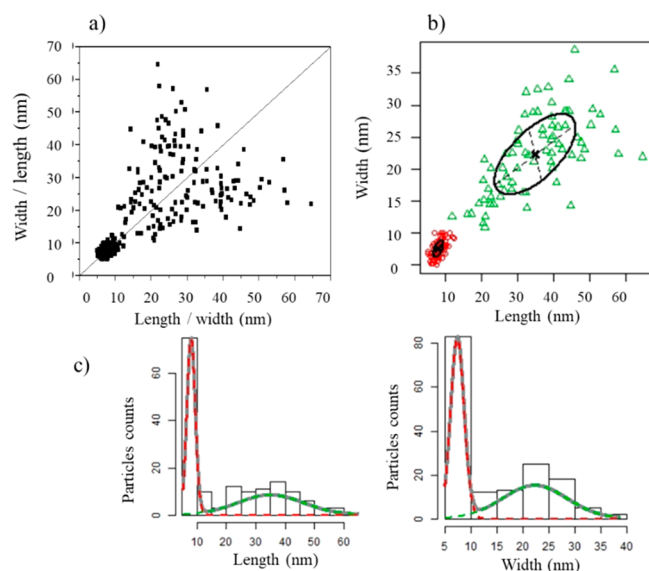


**Figure 3.** (a) 2D plots analysis of length vs width of AgNPs (60 min) deposited on PPF, (b) particles multivariate analysis showing two subpopulations (red dots: isotropic NPs of 8 ( $\pm 1$ ) nm, green dots: anisotropic aggregates of 35 ( $\pm 11$ )  $\times$  22 ( $\pm 6$ ) nm), (c) histograms of particles showing the bimodal distribution.

aggregates of 35 ( $\pm 11$ )  $\times$  22 ( $\pm 6$ ) nm, accounting for 47% of the population, and isotropic NPs of 8 ( $\pm 1$ ) nm, accounting for 53% of the population, are observed (Figure 3b,c, Table 1). It is worth mentioning that the size of AgNPs formed in the supernatant (ca. 5 nm) correlates well with the crystallite size (6 nm) estimated using the Debye–Scherrer equation from the Ag(111) peak at 38.3° of a AgNPs film obtained at  $t = 60$  min (Supporting Information, Figure S8). These experiments confirm that the deposition of Ag NPs on PPF surface by the thermal hydrogenolysis of silver amidinate precursor proceeds similarly to what was already proposed for copper amidinate precursors.<sup>39</sup> The silver deposition mechanism involves the regular nucleation of small Ag NPs in solution and their continuous deposition on the substrate. This process allows a good control of the grafting density of AgNPs on PPF surfaces thanks to the precise modulation of the deposition time.

**Raman Spectra of AgNPs/PPF Surfaces.** Figure 4 shows the Raman spectra of the AgNPs( $t$ )/PPF surfaces. A very distinct behavior is evidenced according to the time of the silver deposition. For short times (1 and 5 min), the Raman spectra are very similar to the bare PPF one. Only wide peaks related to G and D bands of glassy carbon appear at 1600 and 1345  $\text{cm}^{-1}$ , respectively. No extra peak due to the presence of AgNPs is observed. Noticeably, when the AgNPs deposition time reaches 15 and 60 min, an exaltation of the global Raman signal occurs. This effect, called surface enhanced Raman scattering (SERS), appears when electromagnetic interactions

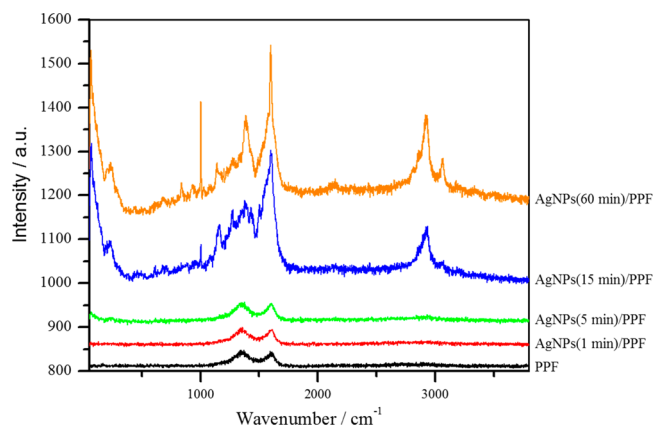


**Figure 4.** Raman spectra of PPF surfaces decorated with silver NPs prepared with different deposition times (1, 5, 15, and 60 min). Laser  $\lambda = 532$  nm.

between very close neighboring silver NPs induce strong localized electric fields in the small gap between the NPs (1 to 2 nm).<sup>49</sup> According to the literature, the electromagnetic amplification effect is maximum just before the percolation threshold of the silver structures on a substrate; that is, when the density of “hot spots” is the highest.<sup>50</sup> In our case, such percolation threshold is reached when the AgNPs/PPF surface coverage is estimated over 51%. At such coverage level, the grafting density of Ag NPs seems to promote interparticle distances small enough to fulfill the plasmonic resonance trapping conditions in the film. The main parameters behind this effect are related to the morphology of plasmonic nanoparticles and their relative distribution within the substrate.<sup>51,52</sup> This exaltation phenomenon is maintained with longer deposition times (60 min). In solution, the surface plasmon of individual AgNPs is usually expected around the value of 400 nm,<sup>8</sup> but due to collective oscillation phenomena of electrons in aggregated NPs, the maximum absorption of the electromagnetic excitation is red shifted toward higher wavelength.<sup>53</sup> Under the 532 nm laser beam, the SERS signal mainly arises from the PPF itself and the organic species present between the aggregated NPs. The G band of PPF is highly exalted by a factor of  $\sim 12$  (by measuring the ratio of peaks height) while being still localized at 1600  $\text{cm}^{-1}$ . The D band seems to be less amplified (factor  $\approx 6$ ) and has slightly shifted from 1345 to  $\sim 1380$   $\text{cm}^{-1}$ . The presence of an extra peak at 1600  $\text{cm}^{-1}$  could be responsible for the apparent higher increase of the G band.

New bands at 245, 1000, 1145, 2930, and 3075  $\text{cm}^{-1}$  are likely originating from organic solvent traces and/or the adsorbed silver metalorganic precursor amidine ligand and/or moieties coming from its decomposition. At this stage, it is difficult to finely attribute these bands to the complex organic moieties that result from the precursor decomposition. To do so, a theoretical simulation of the possible coordinated molecules would be necessary, which is out of the scope of this work.

**Electrochemical Reduction of 4-Nitrophenol at PPF and AgNPs( $t$ )/PPF Surfaces.** Figure 5 shows the electrochemical behavior of the PPF and AgNPs( $t$ )/PPF surfaces for the reduction of 4 NP, chosen as model pollutant. Regardless of the sample, a single irreversible reduction peak is observed by cyclic voltammetry in the potential range of  $-1.0 < E(V) < -0.1$ . This result is in agreement with the ones reported in

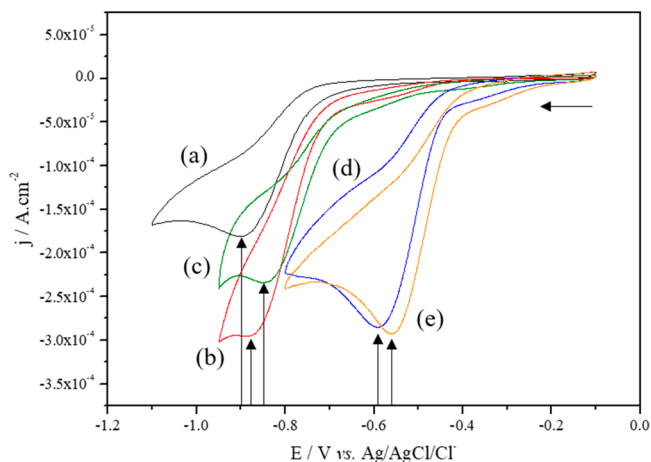


**Figure 5.** CVs recorded on the a) bare PPF (black), b) AgNPs (1 min)/PPF (red); c) AgNPs (15 min)/PPF (d), and AgNPs (60 min)/PPF (e) electrodes in phosphate buffer (0.1 mol L<sup>-1</sup> pH = 7.2); containing 5 × 10<sup>-4</sup> mol·L<sup>-1</sup> 4 NP. Scan rate 0.100 V·s<sup>-1</sup>.

the literature with carbon and/or silver based electrode materials using different electrochemical methods and other supporting electrolytes.<sup>17,22,54–56</sup> At first, CV measurements were performed on two different freshly prepared surfaces of PPF, AgNPs(*t*)/PPF to confirm the reproducibility of the average values of the potential and the current density (fifth cycle) of the reduction peak. The average of the peak potential ( $E_p$ ), the mean size of AgNPs deposited on PPF surfaces, and surface coverage values are summarized Table 1. Two series of samples clearly depend on the deposition time: AgNPs(1 min)/PPF and AgNPs(5 min)/PPF on one hand and AgNPs(15 min)/PPF and AgNPs(60 min)/PPF on the other hand. The relative standard deviation of  $j$  (not shown) and  $E_p$  is below 15% and 3% for all different PPF and AgNPs(*t*)/PPF composite electrodes (excluded first cycle), respectively. These data mean that the PPF electrodes show reproducible results. For short  $t$  values (1 and 5 min), an overall smooth decrease of  $j$  for AgNPs(5 min)/PPF compared to AgNPs(1 min)/PPF is observed while the surface coverage is multiplied by a factor of 2. It is noteworthy that in both cases AgNPs are isotropic with a mean size of 6 (±1) nm and 7 (±2) nm, respectively. For  $t = 1$  min, the AgNPs can be considered isolated enough to avoid the interaction of the diffusion layer. On the contrary, at  $t = 5$  min the distance between the isotropic AgNPs decreases, and an overlap of diffusion zones of neighboring AgNPs occurs. The consequence of this diffusion phenomenon is the decrease of the current density. At  $t = 5$  min, a rupture toward the electron transfer for the reduction of the 4 NP seems to occur. For long  $t$  values (15 and 60 min), neither the size, nor the number of AgNPs, nor the surface coverage are comparable, but the  $j$  values are close. There is a clear evidence that there is a threshold for which the addition of AgNPs does not change the reaction rate. It is well known that AgNPs are catalytically active for the electroreduction of 4 NP.<sup>16,44,56</sup> Consequently, no significant modification of the electroactive surface should be observed. The AgNPs(15 min)/PPF sample appears as the optimum electrode configuration, as it presents a good compromise between the silver amount and the electroreduction rate of 4 NP. The current density increased by a factor of ~2 when comparing the samples with short or long  $t$  values. The simplest explanation would be that the electroactive surface is also

doubled, but the situation is certainly more complex, because the surface coverage is not multiplied by a factor of 2. SEM images and 2D plot analysis of AgNPs deposited on PPF showed, on one hand, larger isotropic AgNPs for  $t = 15$  and  $t = 60$  min than those observed for  $t = 1$  min and  $t = 5$  min (Table 1) and, on the other hand, anisotropic AgNPs exhibiting a similar aspect ratio of 1.4 and 1.6 for  $t = 15$  and 60 min, respectively. The silver nanostructure in terms of size, shape, and distance between the AgNPs clearly influences the electroreduction of 4 NP. We assume that a synergetic effect between AgNPs and carbon PPF surface creates an active nanocomposite interface, which would be responsible for the electrochemical behavior of AgNPs/PPF electrode. Note that the shape of the  $j$ - $E$  curves for PPF electrode and a bare glassy carbon electrode (GCE) in the presence of 4 NP are similar (Supporting Information, Figure S9).<sup>41,57</sup> In addition, the electrochemical behavior of AgNPs(60 min)/PPF and Ag/Si electrodes for the reduction of 4 NP (Supporting Information, Figure S9) is very different. No peak of the reduction of 4 NP is present on the cyclic voltammogram curves for Ag/Si electrode, while a well defined cathodic peak ( $E_p$ ) is present on the CVs for AgNPs (60 min)/PPF sample ( $j = -87.5$  (±13.2)  $\mu\text{A cm}^{-2}$ ,  $E_p = -0.506$  (±0.016) V). These results emphasize the high electrocatalytic behavior of AgNPs(60 min)/PPF toward the reduction of 4 NP, which is directly linked to the silver nanostructure and thus the nanocomposite interface. Indeed, the main difference between AgNPs(60 min)/PPF and Ag/Si is the morphology and size of the silver structure on the PPF and Si surfaces (Figure S10), respectively.

The electrocatalytic behavior toward 4 NP reduction is clearly confirmed by the potential values of the cathodic peak: PPF < AgNPs(1 min) < AgNPs(5 min)/PPF  $\ll$  AgNPs(15 min)/PPF < AgNPs(60 min)/PPF. Moreover, the electrocatalytic properties are also evidenced by comparing the voltammetric behavior of the PPF and AgNPs(*t*)/PPF electrodes in the absence and in the presence of 5 × 10<sup>-4</sup> mol·L<sup>-1</sup> of 4 NP in phosphate buffer solution (Supporting Information Figure S11). It is clearly seen that the current density of the different backgrounds (Figure S11) is much lower than the one of the CVs recorded in the presence of 5 × 10<sup>-4</sup> mol·L<sup>-1</sup> of 4 NP in phosphate buffer solution.

For short time values,  $t = 1$  and 5 min,  $E_p$  values are close to the value of  $E_p$  measured for bare PPF surface, and  $E_p$  values show no variation for  $t = 15$  and 60 min. Remarkably, for  $t = 15$  and 60 min, a total shift of the 4 NP reduction potential,  $\Delta E_p$  (peak to peak difference between  $E_p$  values for PPF and AgNPs(15 min)/PPF or AgNPs(60 min)/PPF), of ~0.33 V is obtained, which is a significant catalytic contribution. This  $\Delta E_p$  value is 1 order of magnitude higher than the one obtained in the case of AgNPs(*t*)/PPF surfaces prepared with short time deposition (1 and 5 min). This reveals that the smallest nanoparticles are not always the most reactive. This surprising catalytic behavior has been already observed for the catalytic activity of 4 NP reduction with NaBH<sub>4</sub> with colloidal AuNPs or AgNPs.<sup>58,59</sup> Its origin is attributed to a combination of many factors among which are the size dependent charge transfer properties of the catalysts and the size dependent chemical interaction between Au catalyst and the 4 NP. In our case, this unexpected electrocatalytic enhancement at  $t = 15$  min could be explained by the AgNPs reactive nanocomposite interface with a high reactivity of silver atoms at the interface of AgNPs and PPF surface (Table 1). Thus, a size and morphology effect



and/or an intercrystalline distance of AgNPs influences the electroactivity, inducing a remarkable decrease of the over potential  $\eta$  needed for the electroreduction of 4 NP.<sup>16</sup> This is very exciting, as it is possible to correlate the strongest electrocatalytic activity of the 4 NP to the onset of the SERS effect on the electrode. The organization of the silver aggregates at the nanoscale is responsible of such combined properties, and it may open the way to cooperative optical and electrochemical characterization for the detection of 4 NP pollutant.

## ■ CONCLUSION

In this work, we have prepared reproducible carbon thin film composite electrodes, with an organometallic deposition of Ag NPs approach. The carbon thin film obtained by the PPF method provides a straightforward way to prepare carbon electrodes exhibiting an electrochemical behavior comparable to glassy carbon electrodes but with reproducible thickness and roughness, avoiding the usually required polishing step. Different silver nanostructures and surface coverage of PPF carbon electrodes were obtained through the hydrogenolysis of the [Ag(Bu amd)] metalorganic precursor, and a remarkable decrease of the overpotential of the reduction of 4 nitrophenol up to 330 mV was measured. Additionally, the substrates having above 51% of their surface covered by Ag NPs showed an SERS effect correlated with an electrocatalytic effect toward the reduction of 4 nitrophenol. These coupled properties may open the route toward devices using a dual optical and electrochemical detection.

## ■ ASSOCIATED CONTENT

### ● Supporting Information

The Supporting Information is available free of charge on the ACS Publications website at DOI: [10.1021/acs.langmuir.9b02405](https://doi.org/10.1021/acs.langmuir.9b02405).

<sup>1</sup>H NMR characterization of the organometallic silver precursor [Ag(Bu amd)], SEM, AFM, and XRD of the PPF surface and SEM of Ag/Si surface. TEM of the supernatant and 2D plots analysis. Comparison of the grazing angle XRD between PPF and AgNPs(60 min)/PPF surfaces. Cyclic voltammograms recorded on the bare PPF; bare glassy carbon, bare PVD Ag/Si and AgNPs(60 min)/PPF electrodes in phosphate buffer solution containing 4 nitrophenol (PDF)

## ■ AUTHOR INFORMATION

### Corresponding Authors

\*E mail: [katia.fajerweg@lcc-toulouse.fr](mailto:katia.fajerweg@lcc-toulouse.fr). (K.F.)

\*E mail: [pierre.fau@lcc-toulouse.fr](mailto:pierre.fau@lcc-toulouse.fr). (P.F.)

### ORCID

Maxime Puyo: 0000 0001 9662 3293

Pierre Fau: 0000 0003 0014 2511

Myrtil L. Kahn: 0000 0003 3079 5759

David Mesguich: 0000 0002 4479 1292

Katia Fajerweg: 0000 0002 3897 3380

### Notes

The authors declare no competing financial interest.

## ■ ACKNOWLEDGMENTS

This work was partially supported by LAAS CNRS micro/nanotechnologies platform, member of the French RENA

TECH network. The authors wish to acknowledge the financial support of the Centre National de la Recherche Scientifique (CNRS) and the Ministère de l'Enseignement Supérieur, de la Recherche et de l'Innovation (MESRI). The authors acknowledge V. Collière, M. Tessier, L. Vendier, S. Mallet Ladeira, and A. Sournia Saquet, for their precious help in SEM FEG, AFM, XRD, and electrochemistry measurements, respectively. N. Jaffrezic and C. Trupin were very helpful for the conception and the fabrication of the PEEK microcell for electrochemistry measurements.

## ■ REFERENCES

- (1) Choi, S.; Han, S. I.; Kim, D.; Hyeon, T.; Kim, D. H. High performance stretchable conductive nanocomposites: materials, processes, and device applications. *Chem. Soc. Rev.* 2019, 48 (6), 1566–1595.
- (2) Kanti Das, T.; Ganguly, S.; Remanan, S.; Das, N. C. Temperature Dependent Study of Catalytic Ag Nanoparticles Entrapped Resin Nanocomposite towards Reduction of 4 Nitro phenol. *ChemistrySelect* 2019, 4 (13), 3665–3671.
- (3) Kao, J.; Thorkelsson, K.; Bai, P.; Rancatore, B. J.; Xu, T. Toward functional nanocomposites: taking the best of nanoparticles, polymers, and small molecules. *Chem. Soc. Rev.* 2013, 42 (7), 2654–2678.
- (4) Nethravathi, C.; Anumol, E. A.; Rajamathi, M.; Ravishankar, N. Highly dispersed ultrafine Pt and PtRu nanoparticles on graphene: formation mechanism and electrocatalytic activity. *Nanoscale* 2011, 3 (2), 569–71.
- (5) Xiao, Y.; Li, C. M. Nanocomposites: from fabrications to electrochemical bioapplications. *Electroanalysis* 2008, 20 (6), 648–662.
- (6) Garrett, D. J.; Brooksby, P. A.; Rawson, F. J.; Baronian, K. H. R.; Downard, A. J. Reproducible Fabrication of Robust, Renewable Vertically Aligned Multiwalled Carbon Nanotube/Epoxy Composite Electrodes. *Anal. Chem. (Washington, DC, U. S.)* 2011, 83 (21), 8347–8351.
- (7) Devi, L. B.; Mandal, A. B. Self assembly of Ag nanoparticles using hydroxypropyl cyclodextrin. Synthesis, characterisation and application for the catalytic reduction of p nitrophenol. *RSC Adv.* 2013, 3 (15), 5238–5253.
- (8) Cure, J.; Coppel, Y.; Dammak, T.; Fazzini, P. F.; Mlayah, A.; Chaudret, B.; Fau, P. Monitoring the Coordination of Amine Ligands on Silver Nanoparticles Using NMR and SERS. *Langmuir* 2015, 31 (4), 1362–1367.
- (9) Fernandez Merino, M. J.; Guardia, L.; Paredes, J. I.; Villar Rodil, S.; Martinez Alonso, A.; Tascon, J. M. D. Developing green photochemical approaches towards the synthesis of carbon nanofiber and graphene supported silver nanoparticles and their use in the catalytic reduction of 4 nitrophenol. *RSC Adv.* 2013, 3 (40), 18323–18331.
- (10) Zhang, Z.; Shao, C.; Sun, Y.; Mu, J.; Zhang, M.; Zhang, P.; Guo, Z.; Liang, P.; Wang, C.; Liu, Y. Tubular nanocomposite catalysts based on size controlled and highly dispersed silver nanoparticles assembled on electrospun silica nanotubes for catalytic reduction of 4 nitrophenol. *J. Mater. Chem.* 2012, 22 (4), 1387–1395.
- (11) Sun, Y.; Xia, Y. Shape Controlled Synthesis of Gold and Silver Nanoparticles. *Science (Washington, DC, U. S.)* 2002, 298 (5601), 2176–2179.
- (12) Campbell, F. W.; Compton, R. G. The use of nanoparticles in electroanalysis: an updated review. *Anal. Bioanal. Chem.* 2010, 396 (1), 241–259.
- (13) Cao, H. L.; Huang, H. B.; Chen, Z.; Karadeniz, B.; Lu, J.; Cao, R. Ultrafine Silver Nanoparticles Supported on a Conjugated Microporous Polymer as High Performance Nanocatalysts for Nitro phenol Reduction. *ACS Appl. Mater. Interfaces* 2017, 9 (6), 5231–5236.
- (14) Dector, A.; Arjona, N.; Guerra Balcazar, M.; Esquivel, J. P.; Del Campo, F. J.; Sabate, N.; Ledesma Garcia, J.; Arriaga, L. G. Non

Conventional Electrochemical Techniques for Assembly of Electrodes on Glassy Carbon Like PPF Materials and Their Use in a Glucose Microfluidic Fuel Cell. *Fuel Cells (Weinheim, Ger.)* **2014**, *14* (6), 810–817.

(15) Polsky, R.; Washburn, C. M.; Montano, G.; Liu, H.; Edwards, T. L.; Lopez, D. M.; Harper, J. C.; Brozik, S. M.; Wheeler, D. R. Reactive Ion Etching of Gold Nanoparticle Modified Pyrolyzed Photoresist Films. *Small* **2009**, *5* (22), 2510–2513.

(16) Casella, I. G.; Contursi, M. The Electrochemical Reduction of Nitrophenols on Silver Globular Particles Electrodeposited under Pulsed Potential Conditions. *J. Electrochem. Soc.* **2007**, *154* (12), D697–D702.

(17) Zhang, C.; Govindaraju, S.; Giribabu, K.; Huh, Y. S.; Yun, K. AgNWs PANI nanocomposite based electrochemical sensor for detection of 4 nitrophenol. *Sens. Actuators, B* **2017**, *252*, 616–623.

(18) Ikhsan, N. I.; Rameshkumar, P.; Huang, N. M. Electrochemical properties of silver nanoparticle supported reduced graphene oxide in nitric oxide oxidation and detection. *RSC Adv.* **2016**, *6* (108), 107141–107150.

(19) Esumi, K.; Isono, R.; Yoshimura, T. Preparation of PAMAM and PPI Metal (Silver, Platinum, and Palladium) Nanocomposites and Their Catalytic Activities for Reduction of 4 Nitrophenol. *Langmuir* **2004**, *20* (1), 237–243.

(20) Lopez Salido, I.; Lim, D. C.; Kim, Y. D. Ag nanoparticles on highly ordered pyrolytic graphite (HOPG) surfaces studied using STM and XPS. *Surf. Sci.* **2005**, *588* (1–3), 6–18.

(21) Zhang, P.; Shao, C.; Zhang, Z.; Zhang, M.; Mu, J.; Guo, Z.; Liu, Y. In situ assembly of well dispersed Ag nanoparticles (AgNPs) on electrospun carbon nanofibers (CNFs) for catalytic reduction of 4 nitrophenol. *Nanoscale* **2011**, *3* (8), 3357–3363.

(22) Ikhsan, N. I.; Rameshkumar, P.; Huang, N. M. Controlled synthesis of reduced graphene oxide supported silver nanoparticles for selective and sensitive electrochemical detection of 4 nitrophenol. *Electrochim. Acta* **2016**, *192*, 392–399.

(23) Koh, S. J. Strategies for controlled placement of nanoscale building blocks. *Nanoscale Res. Lett.* **2007**, *2* (11), 519–545.

(24) Cure, J.; Assi, H.; Cocq, K.; Marin, L.; Fajerweg, K.; Fau, P.; Beche, E.; Chabal, Y. J.; Esteve, A.; Rossi, C. Controlled Growth and Grafting of High Density Au Nanoparticles on Zinc Oxide Thin Films by Photo Deposition. *Langmuir* **2018**, *34* (5), 1932–1940.

(25) Liu, S.; Wang, X.; Zhang, S.; Lu, X.; Li, T.; Pang, F.; Chen, Z.; Chen, N. The fabrication of a high sensitivity surface enhanced Raman spectra substrate using texturization and electroplating technology. *Appl. Surf. Sci.* **2019**, *490*, 109–116.

(26) Shen, S. C.; Liu, W. T.; Diao, J. J. Colloidally deposited nanoparticle wires for biophysical detection. *Chin. Phys. B* **2015**, *24* (12), 127308.

(27) Stetsenko, M. O.; Rudenko, S. P.; Maksimenko, L. S.; Serdega, B. K.; Pluchery, O.; Snegir, S. V. Optical Properties of Gold Nanoparticle Assemblies on a Glass Surface. *Nanoscale Res. Lett.* **2017**, *12* (1), 1–10.

(28) Fajerweg, K.; Ynam, V.; Chaudret, B.; Garcon, V.; Thouron, D.; Comtat, M. An original nitrate sensor based on silver nanoparticles electrodeposited on a gold electrode. *Electrochem. Commun.* **2010**, *12* (10), 1439–1441.

(29) Supur, M.; Smith, S. R.; McCreery, R. L. Characterization of Growth Patterns of Nanoscale Organic Films on Carbon Electrodes by Surface Enhanced Raman Spectroscopy. *Anal. Chem. (Washington, DC, U. S.)* **2017**, *89* (12), 6463–6471.

(30) Cruickshank, A. C.; Downard, A. J. Electrochemical stability of citrate capped gold nanoparticles electrostatically assembled on amine modified glassy carbon. *Electrochim. Acta* **2009**, *54* (23), 5566–5570.

(31) Michel, R. R. I.; Sutherland, D.; Fokas, C.; Csucs, G.; Danuser, G.; Spencer, N. D.; Textor, M.; et al. A Novel Approach To Produce Biologically Relevant Chemical Patterns at the Nanometer Scale: Selective Molecular Assembly Patterning Combined with Colloidal Lithography. *Langmuir* **2002**, *18* (22), 8580–8586.

(32) Schlichthaerle, T.; Strauss, M. T.; Schueder, F.; Woehrstein, J. B.; Jungmann, R. DNA nanotechnology and fluorescence applications. *Curr. Opin. Biotechnol.* **2016**, *39*, 41–47.

(33) Breton, T.; Downard, A. J. Controlling Grafting from Aryldiazonium Salts: A Review of Methods for the Preparation of Monolayers. *Aust. J. Chem.* **2017**, *70* (9), 960–972.

(34) Downard, A. J.; Garrett, D. J.; Tan, E. S. Q. Microscale Patterning of Organic Films on Carbon Surfaces Using Electrochemistry and Soft Lithography. *Langmuir* **2006**, *22* (25), 10739–10746.

(35) Lee, L.; Brooksby, P. A.; Downard, A. J. The stability of diazonium ion terminated films on glassy carbon and gold electrodes. *Electrochem. Commun.* **2012**, *19*, 67–69.

(36) Menanteau, T.; Dias, M.; Levillain, E.; Downard, A. J.; Breton, T. Electrografting via diazonium chemistry: key role of aryl substituent in layer growth mechanism. *J. Phys. Chem. C* **2016**, *120* (8), 4423–4429.

(37) Coperet, C.; Fedorov, A.; Zhizhko, P. A. Surface Organometallic Chemistry: Paving the Way Beyond Well Defined Supported Organometallics and Single Site Catalysis. *Catal. Lett.* **2017**, *147* (9), 2247–2259.

(38) Xu, Z.; Xu, R.; Yue, Y.; Yuan, P.; Bao, X.; Abou Hamad, E.; Basset, J. M.; Zhu, H. Bimetallic Pt Sn nanocluster from the hydrogenolysis of a well defined surface compound consisting of [(AlO)Pt(COD)Me] and [(AlO)SnPh<sub>3</sub>] fragments for propane dehydrogenation. *J. Catal.* **2019**, *374*, 391–400.

(39) Cure, J.; Piettre, K.; Sournia Saquet, A.; Coppel, Y.; Esvan, J.; Chaudret, B.; Fau, P. A Novel Method for the Metalization of 3D Silicon Induced by Metastable Copper Nanoparticles. *ACS Appl. Mater. Interfaces* **2018**, *10* (38), 32838–32848.

(40) Lebon, E.; Fau, P.; Comtat, M.; Kahn, M. L.; Sournia Saquet, A.; Temple Boyer, P.; Dubreuil, B.; Behra, P.; Fajerweg, K. In Situ Metalorganic Deposition of Silver Nanoparticles on Gold Substrate and Square Wave Voltammetry: A Highly Efficient Combination for Nanomolar Detection of Nitrate Ions in Sea Water. *Chemosensors* **2018**, *6* (4), 50.

(41) McCreery, R. L. Advanced Carbon Electrode Materials for Molecular Electrochemistry. *Chem. Rev. (Washington, DC, U. S.)* **2008**, *108* (7), 2646–2687.

(42) Brooksby, P. A.; Downard, A. J. Electrochemical and atomic force microscopy study of carbon surface modification via diazonium reduction in aqueous and acetonitrile solutions. *Langmuir* **2004**, *20* (12), 5038–45.

(43) Downard, A. J.; Tan, E. S. Q.; Yu, S. S. C. Controlled assembly of gold nanoparticles on carbon surfaces. *New J. Chem.* **2006**, *30* (9), 1283–1288.

(44) Barman, K.; Changmai, B.; Jasimuddin, S. Electrochemical Detection of Para nitrophenol using Copper Metal Nanoparticles Modified Gold Electrode. *Electroanalysis* **2017**, *29* (12), 2780–2787.

(45) Ounnunkad, K.; Patten, H. V.; Velicky, M.; Farquhar, A. K.; Brooksby, P. A.; Downard, A. J.; Dryfe, R. A. W. Electrowetting on conductors: anatomy of the phenomenon. *Faraday Discuss.* **2017**, *199*, 49–61.

(46) Zhao, Z.; Zheng, Z.; Roux, C.; Delmas, C.; Marty, J. D.; Kahn, M. L.; Mingotaud, C. Importance of the Correlation between Width and Length in the Shape Analysis of Nanorods: Use of a 2D Size Plot To Probe Such a Correlation. *Chem. Eur. J.* **2016**, *22* (35), 12424–12429.

(47) Kostecki, R.; Schnyder, B.; Alliata, D.; Song, X.; Kinoshita, K.; Kotz, R. Surface studies of carbon films from pyrolyzed photoresist. *Thin Solid Films* **2001**, *396*, 36–43.

(48) Ferrari, A. C.; Libassi, A.; Tanner, B. K.; Stolojan, V.; Yuan, J.; Brown, L. M.; Rodil, S. E.; Kleinsorge, B.; Robertson, J. Density, sp<sup>3</sup> fraction, and cross sectional structure of amorphous carbon films determined by x ray reflectivity and electron energy loss spectroscopy. *Phys. Rev. B: Condens. Matter Mater. Phys.* **2000**, *62* (16), 11089–11103.

- (49) Romero, I.; Aizpurua, J.; Bryant, G. W.; Garcia De Abajo, F. J. Plasmons in nearly touching metallic nanoparticles: singular response in the limit of touching dimers. *Opt. Express* **2006**, *14* (21), 9988–99.
- (50) Metin Akinoglu, E.; Sun, T.; Gao, J.; Giersig, M.; Ren, Z.; Kempa, K. Evidence for critical scaling of plasmonic modes at the percolation threshold in metallic nanostructures. *Appl. Phys. Lett.* **2013**, *103* (17), 171106.
- (51) Langer, J.; Novikov, S. M.; Liz Marzan, L. M. Sensing using plasmonic nanostructures and nanoparticles. *Nanotechnology* **2015**, *26* (32), 1–28.
- (52) Reguera, J.; Langer, J.; Jimenez de Aberasturi, D.; Liz Marzan, L. M. Anisotropic metal nanoparticles for surface enhanced Raman scattering. *Chem. Soc. Rev.* **2017**, *46* (13), 3866–3885.
- (53) Gunnarsson, L.; Rindzevicius, T.; Prikulis, J.; Kasemo, B.; Kall, M.; Zou, S.; Schatz, G. C. Confined plasmons in nanofabricated single silver particle pairs: experimental observations of strong interparticle interactions. *J. Phys. Chem. B* **2005**, *109* (3), 1079–1087.
- (54) Danhel, A.; Mansfeldova, V.; Janda, P.; Vyskocil, V.; Barek, J. Crystalline silver amalgam a novel electrode material. *Analyst (Cambridge, U. K.)* **2011**, *136* (18), 3656–3662.
- (55) Fischer, J.; Vanourkova, L.; Danhel, A.; Vyskocil, V.; Cizek, K.; Barek, J.; Peckova, K.; Yosypchuk, B.; Navratil, T. Voltammetric determination of nitrophenols at a silver solid amalgam electrode. *Int. J. Electrochem. Sci.* **2007**, *2* (3), 226–234.
- (56) Madhu, R.; Karuppiyah, C.; Chen, S. M.; Veerakumar, P.; Liu, S. B. Electrochemical detection of 4 nitrophenol based on biomass derived activated carbons. *Anal. Methods* **2014**, *6* (14), 5274–5280.
- (57) Brooksby, P. A.; Downard, A. J. Nanoscale Patterning of Flat Carbon Surfaces by Scanning Probe Lithography and Electrochemistry. *Langmuir* **2005**, *21* (5), 1672–1675.
- (58) Fenger, R.; Fertitta, E.; Kirmse, H.; Thuenemann, A. F.; Rademann, K. Size dependent catalysis with CTAB stabilized gold nanoparticles. *Phys. Chem. Chem. Phys.* **2012**, *14* (26), 9343–9349.
- (59) Piella, J.; Merkoci, F.; Genc, A.; Arbiol, J.; Bastus, N. G.; Puntès, V. Probing the surface reactivity of nanocrystals by the catalytic degradation of organic dyes: the effect of size, surface chemistry and composition. *J. Mater. Chem. A* **2017**, *5* (23), 11917–11929.